Article

Influence of Supports on the Catalytic Activity and Coke Resistance of Ni Catalyst in Dry Reforming of Methane

Da Hye Song [1,2], Un Ho Jung [1], Young Eun Kim [1,2], Hyo Been Im [1], Tae Ho Lee [1], Ki Bong Lee [2,*] and Kee Young Koo [1,3,*]

1. Hydrogen Research Department, Korea Institute of Energy Research, 152 Gajeong-ro, Yuseong-gu, Daejeon 34129, Korea; sdh8908@kier.re.kr (D.H.S.); uhjung@kier.re.kr (U.H.J.); kyes1258@kier.re.kr (Y.E.K.); iyb2001@kier.re.kr (H.B.I.); thl9007@kier.re.kr (T.H.L.)
2. Department of Chemical and Biological Engineering, Korea University, 145 Anam-ro, Seongbuk-gu, Seoul 02841, Korea
3. Advanced Energy and System Engineering, University of Science and Technology (UST), 217 Gajeong-ro, Yuseong-gu, Daejeon 34113, Korea
* Correspondence: kibonglee@korea.ac.kr (K.B.L.); kykoo@kier.re.kr (K.Y.K.); Tel.: +82-2-3290-4851 (K.B.L.); +82-42-860-3192 (K.Y.K.)

Abstract: The dependence of the catalytic activity and coke resistance of Ni-based catalysts on the support type was investigated in the dry reforming of methane (DRM). Catalysts were prepared using incipient wetness impregnation and analyzed using ICP-OES, BET-BJH, XRD, H_2-chemisorption, H_2-TPR, and CO_2-TPD. DRM was performed at 600–750 °C at 144,000 mL/g_{cat}·h of GHSV (CH_4/CO_2/N_2 = 1/1/1). Ni/Al_2O_3 and Ni/MgO catalysts formed $NiAl_2O_4$ and NiO-MgO solid solutions, respectively, owing to strong binding between the metal and support. In contrast, MgO-Al_2O_3 and $MgAl_2O_4$ supports suppressed $NiAl_2O_4$ and NiO-MgO solid solution formation, due to Mg addition, with high metal dispersions of 4.6 and 6.6%, respectively. In the DRM reaction, the Ni/MgO-Al_2O_3 and Ni/$MgAl_2O_4$ catalysts showed high CH_4 conversions of 78.1 and 76.8%, respectively, compared with Ni/Al_2O_3 and Ni/MgO at 750 °C. A stability test was performed at 600 °C for 20 h. A coke study of the spent catalysts was performed using SEM and TGA. Alkaline-earth metal-containing catalysts Ni/MgO-Al_2O_3 and Ni/$MgAl_2O_4$ with strong CO_2 adsorption properties showed 20 wt% reduction in carbon deposition compared to commercial catalysts. Therefore, the support and basic properties of the catalyst significantly influenced the catalyst performance and coke resistance in the DRM.

Keywords: dry reforming of methane; syngas; coke resistance; Ni catalyst; MgO-Al_2O_3

1. Introduction

Recently, there has been an increased focus on problems related to climate change and the need for reducing carbon dioxide (CO_2) emissions. The development of carbon dioxide utilization (CDU) technologies is necessary to reduce CO_2 emissions over the long term. Among CDU technologies, the dry reforming of methane (DRM) reaction is an important technique that could be used to reduce the total annual anthropogenic greenhouse gas emissions (multi-Gt_{CO2}/year) [1,2]. An advantage of the DRM reaction is its low operational cost, as it does not require complicated gas separation [3]. The DRM reaction (Equation (1)) produces the beneficial syngas (H_2 + CO) from CH_4 and CO_2 [4]. Syngas is a raw material for high value-added chemicals, such as oxo-alcohol, formaldehyde, and methanol. Notably, the product H_2/CO ratio of the DRM reaction is 1, which renders the produced syngas suitable for the synthesis of methanol and dimethyl ether or Fischer–Tropsch synthesis [5]. The DRM reaction is strongly endothermic [6] and proceeds at a relatively high temperature (650–850 °C) [7]. The reverse water gas shift (RWGS) reaction (Equation (2)) occurs as a side reaction up to 820 °C under the DRM

reaction conditions, due to the endothermic nature of the reaction. Since the RWGS reaction produces CO and H_2O using CO_2 and H_2, the H_2/CO ratio is lower than 1.

$$CH_4 + CO_2 \rightarrow 2H_2 + 2CO \ (\Delta H_{298K} = +247 \ kJ/mol) \tag{1}$$

$$CO_2 + H_2 \rightarrow H_2O + CO \ (\Delta H_{298K} = +41 \ kJ/mol) \tag{2}$$

$$CH_4 \rightarrow 2H_2 + C \ (\triangle H_{298K} = +74.9 \ kJ/mol) \tag{3}$$

$$2CO \rightarrow CO_2 + C \ (\triangle H_{298K} = -172.4 \ kJ/mol) \tag{4}$$
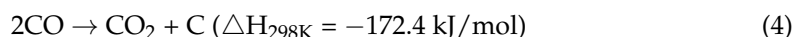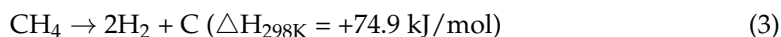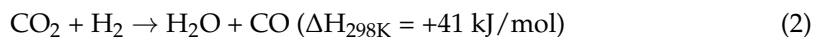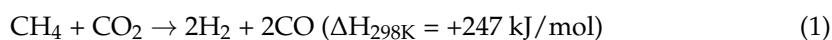
Ni-based catalysts are the most widely used in the DRM reaction because of their high activity and low cost [8]. However, they can cause catalyst deactivation due to processes such as carbon deposition and sintering. Moreover, they have been reported to have three phases: Ni metallic state, Ni oxide, and Ni carbide phase, which influence carbon deposition. Among these, Ni metal atoms of the Ni carbide phase bind strongly with carbon; thus, easily causing carbon deposition [9]. In addition, at high reaction temperatures the active metal forms aggregates, owing to the sintering effect. The agglomeration of particles occurs randomly, causing low metal dispersion and low specific surface area at high temperatures. Moreover, the DRM reaction is more vulnerable to carbon deposition because of the higher carbon ratio in the reactants compared with other methane reforming reactions. Carbon deposition mainly occurs through CH_4 decomposition (Equation (3)) and CO disproportionation (Equation (4)) reactions. As CH_4 decomposition is endothermic, it mainly occurs above 557 °C, whereas the CO disproportionation reaction occurs below 700 °C, due to the exothermic nature of the reaction. Therefore, carbon deposition occurs in the temperature range of 557–700 °C [10]. The morphology of carbon exhibits variations in properties, which cause differences in the activity of the catalyst. In particular, filamentous carbon influences catalyst deactivation during the DRM reaction. Filamentous carbon is formed through diffusion, nucleation, and growth through Ni particles at temperatures > 450 °C. While filamentous carbon does not block the active sites of the Ni metal, it causes catalyst destruction and a pressure drop, due to pore plugging [11]. For this reason, the DRM reaction has limited commercial viability. In this context, the development of catalysts with high catalytic activity and coke resistance in the DRM reaction is essential.

In the preparation of DRM reaction catalysts, the type of support used has a significant influence on the catalytic activity. Among the various supports used in the DRM reaction, Zhang et al. reported that a ZrO_2 support had a low metal dispersion, owing to its low specific surface area of 30 m^2/g, and also had a weak interaction between NiO and the support [12]. Whereas, amorphous ZrO_2 showed a high specific surface area of 200–300 m^2/g and had weak thermal stability. However, a tetragonal phase was formed by calcination at temperatures above 450 °C, which remained stable at high temperatures, owing to its strong thermal stability [13]. Depending on the calcination temperature used, Al_2O_3 supports are divided into α-Al_2O_3, θ-Al_2O_3, and γ-Al_2O_3. In comparison to other Al_2O_3 supports, the γ-Al_2O_3 support has high catalytic activity and anti-coking properties, owing to its smaller particle size [14]. In the Ni/γ-Al_2O_3 catalyst, relatively fine Ni particles are formed, owing to the high specific surface area of γ-Al_2O_3. However, $NiAl_2O_4$ forms a spinel structure during the heat treatment process. The high thermal stability of $NiAl_2O_4$ spinel results in an increase in the reduction temperature and a reduction in the number of active sites, owing to the low metal dispersion [12]. The MgO support has a low specific surface area and forms a NiO-MgO solid solution in the presence of the Ni catalyst, which limits reduction and causes low metal dispersion [15]. In contrast, the MgO support enhances the adsorption of acidic CO_2 gas, owing to the basic properties of MgO. As the adsorbed CO_2 releases oxygen species upon dissociation, the MgO support enhances the coke resistance by promoting the oxidation of carbon formed on the catalyst surface [16,17]. In addition, owing to the basic properties of the Mg-Al mixed oxide support, the Mg-Al mixed oxide support improves the amount of CO_2 adsorption, compared with the Al_2O_3 support [18]. A Mg-Al mixed oxide has a layered double hydroxide (LDH) structure, in which ion exchange between the cation

and anion layers is possible. The Mg^{2+} and Al^{3+} ions are uniformly dispersed between the hydroxide layers, therefore the LDH structure can effectively disperse the nanoparticles, without particle agglomeration. In addition, the $MgO-Al_2O_3$ (LDH) support is transformed into a spinel structure during the heat treatment process and has high thermal stability. In particular, $MgO-Al_2O_3$ as a support for a Ni catalyst suppresses the formation of the $NiAl_2O_4$ and NiO-MgO solid solution, which is advantageous for high metal dispersion, owing to its large specific surface area [12,17]. Moreover, highly dispersed active metals on the $MgO-Al_2O_3$ support have strong metal-support interactions (SMSIs). Consequently, the sintering effect is inhibited [19,20].

Ni-based catalysts have a low coke resistance, but can improve the catalytic activity and durability by dispersing the active metals or enhancing their basic properties [21]. The γ-Al_2O_3 support has a large specific surface and forms fine particles, while the MgO support has excellent basic properties. The bimetallic $MgO-Al_2O_3$ and $MgAl_2O_4$ supports can, thus, overcome the disadvantages of the γ-Al_2O_3 and MgO supports. Therefore, in this study, the influence of various supports: γ-Al_2O_3, MgO, $MgO-Al_2O_3$, and $MgAl_2O_4$, was evaluated to improve the catalytic activity and coke resistance of Ni-based catalysts for the DRM reaction. In addition, the prepared catalysts were compared with commercial catalysts (Ni/Al_2O_3 and $Ni/CaAl_2O_4$) in the dry reforming of methane (DRM) reaction.

2. Results and Discussion

2.1. Characteristics

The characteristics of the catalysts are listed in Table 1. The Ni metal content of the catalysts was confirmed using ICP-OES analysis. The loading amounts of the prepared and commercial catalysts were approximately 10 and 15 wt%, respectively. Ni-based catalysts have a reduced specific surface area compared to that of the fresh support, due to the pore-blocking during the process of preparing the supported Ni metals. In particular, the Ni/MgO catalyst exhibited a significant decrease in the specific surface area of 17.7 m^2/g after the Ni metal was supported. Zanganeh et al. reported that the crystallite size increased and the specific surface area decreased with increasing calcination temperature when NiO-MgO was calcined at 600–800 °C [22]. The $Ni/MgAl_2O_4$ catalyst maintained a relatively high specific surface area of 113.3 m^2/g. Since the $Ni/MgO-Al_2O_3$ catalyst exhibited changes in the textural properties of the $MgO-Al_2O_3$ support during the heat treatment, its specific surface area was lower by 108.7 m^2/g, compared to that of the $Ni/MgAl_2O_4$ catalyst. This was attributed to the lack of calcination of the $MgO-Al_2O_3$ (LDH) support used for the Ni catalyst preparation, which contained MgO and Al_2O_3 in a 30:70 (wt%) ratio. Among the prepared Ni-based catalysts, the Ni/Al_2O_3 catalyst had the lowest metal dispersion of 2.1%, and the metal dispersion of the Ni/MgO catalyst could not be measured because of the high reduction temperature. The $Ni/MgO-Al_2O_3$ catalyst, which exhibited changes in the textural properties of the support during heat treatment, showed a lower metal dispersion (4.6%) than the $Ni/MgAl_2O_4$ catalyst (6.6%). In addition, the commercial catalysts had very low metal dispersions, of less than 0.5%, compared those of the prepared catalysts.

**Table 1.** Characteristics of supports and Ni-based catalysts.

	Ni Content (wt%)	Specific Surface Area [1] (m^2/g)	Metal Dispersion [2] (%)	H$_2$ Uptake [3] (μmol/g)	CO$_2$ Desorption Amount [4] (μmol/g)
Al$_2$O$_3$		132.2			
MgO		124.0			
MgO-Al$_2$O$_3$	-	177.6	-	-	-
MgAl$_2$O$_4$		135.1			
Ni/Al$_2$O$_3$	9.2	103.5	2.1	94	26
Ni/MgO	9.2	17.7	N/A[5]	39	170
Ni/MgO-Al$_2$O$_3$	8.9	108.7	4.6	98	110
Ni/MgAl$_2$O$_4$	9.1	113.3	6.6	96	125
Commercial A	15.6	3.7	0.4	105	9
Commercial B	15.9	24.6	0.5	182	81

[1] Estimated from N$_2$ adsorption at −196 °C. [2] Estimated from H$_2$-Chemisorption at 50 °C. [3] Estimated from H$_2$-TPR in the temperature range 30–1000 °C. [4] Estimated from CO$_2$-TPD analysis in the temperature range 50–800 °C. [5] N/A: Not available.

The composition and crystalline phases of the catalysts were confirmed by XRD analysis. XRD patterns are shown in Figure 1. The Ni/Al$_2$O$_3$ catalyst formed a NiAl$_2$O$_4$ spinel crystalline phase. Nurunnabi et al. reported that the NiO peak shifted from 2θ = 43.26° to 2θ = 42.90–43.00° with the formation of a NiO-MgO solid solution [23]. The NiO peak of the prepared Ni/MgO catalyst also shifted to 2θ = 42.76°, owing to the formation of the NiO-MgO solid solution. In particular, Ni/MgO-Al$_2$O$_3$, Ni/MgAl$_2$O$_4$ catalysts displayed peaks corresponding to MgAl$_2$O$_4$ and NiO, and those corresponding to the NiAl$_2$O$_4$ and NiO-MgO solid solutions were not detected. The catalysts without alkaline earth metals presented peaks of NiAl$_2$O$_4$, but the Ca-containing commercial catalyst B showed a reduced formation of NiAl$_2$O$_4$ compared with catalysts using Al$_2$O$_3$ as a support. Therefore, the addition of alkaline earth metals effectively suppressed the formation of NiAl$_2$O$_4$ and NiO-MgO solid solutions.
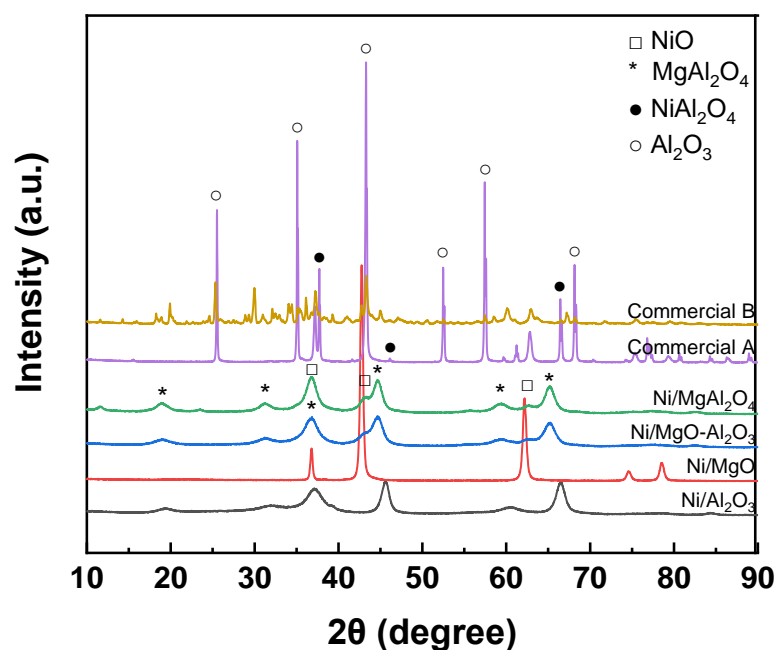
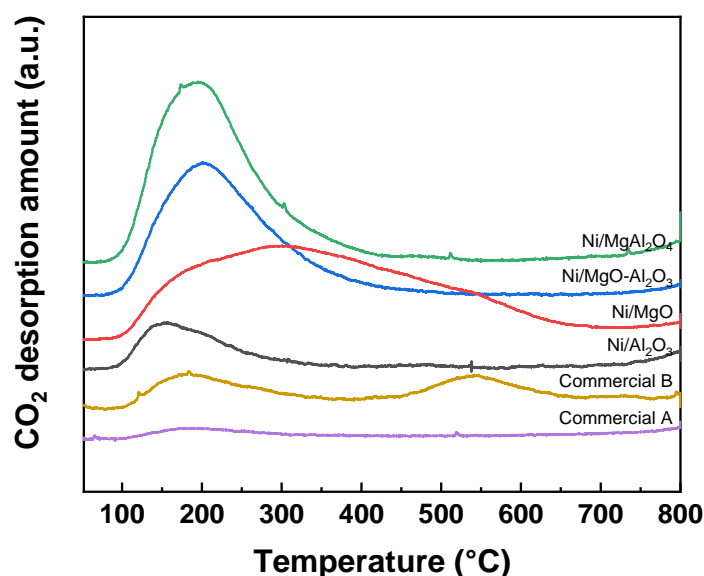**Figure 1.** XRD patterns of Ni catalysts with various supports.

H$_2$-TPR analysis was conducted to analyze the reducibility of the catalysts (Figure 2). Pure NiO (unsupported) can be reduced in the 300–550 °C temperature range, while pure NiAl$_2$O$_4$ (unsupported) was reduced in the 730–900 °C temperature range [24,25]. In addition, a reduction peak associated with surface NiO weak interactions was formed in the temperature range of 500–550 °C, while the reduction peak formed in the temperature range of 700–800 °C was attributed to strong interactions between NiO and the support [26,27]. As bulk NiO has a weak interaction with the support, bulk NiO was mainly reduced at 250–500 °C [28]. A peak corresponding to the reduction of the commercial catalyst A was observed at 300–500 °C. The reduction peak corresponding to the commercial catalyst B was observed at 400–800 °C. Therefore, commercial catalysts were confirmed to have NiO with relatively weak interactions and bulk NiO. As confirmed by the XRD results, the Ni/Al$_2$O$_3$ catalyst, which was difficult to reduce due to the formation of NiAl$_2$O$_4$, underwent reduction at temperatures above 900 °C. In particular, because the Ni/MgO catalyst formed a stable NiO-MgO solid solution, the Ni/MgO catalyst was resistant to reduction up to 1000 °C. The Ni/MgO-Al$_2$O$_3$ and Ni/MgAl$_2$O$_4$ catalysts were mainly reduced at 800 °C. As the Ni/MgO-Al$_2$O$_3$ and Ni/MgAl$_2$O$_4$ catalysts had SMSIs, the Ni active metals were highly dispersed, and both Ni/MgO-Al$_2$O$_3$ and Ni/MgAl$_2$O$_4$ were reduced at higher temperatures compared to the commercial catalysts. In addition, because the Ni/MgO-Al$_2$O$_3$ and Ni/MgAl$_2$O$_4$ catalysts had a stable spinel structure (MgAl$_2$O$_4$) after calcination, the formation of NiAl$_2$O$_4$ or NiO-MgO solid solutions was suppressed. Therefore, the Ni/MgO-Al$_2$O$_3$ and Ni/MgAl$_2$O$_4$ catalysts displayed improved reducibility compared to the Ni/Al$_2$O$_3$ and Ni/MgO catalysts.
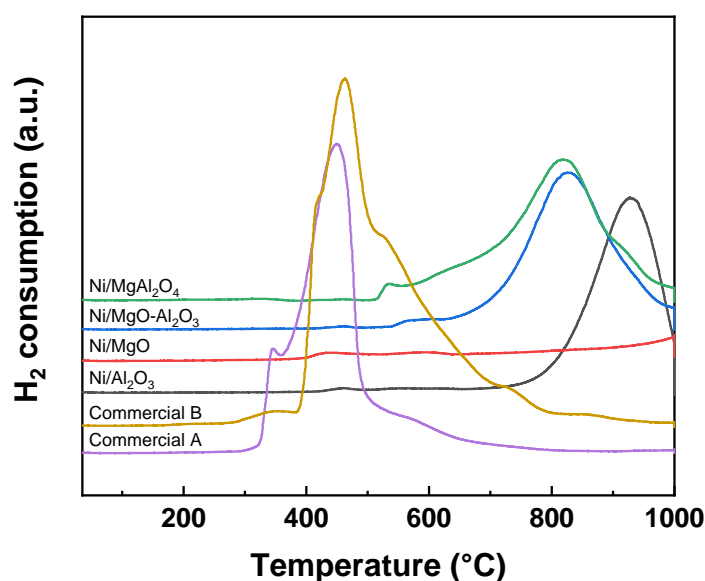
Figure 2. H$_2$-TPR profiles of Ni catalysts with various supports.

CO$_2$-TPD analysis was conducted to determine the basic properties of the catalysts (Figure 3). In general, the catalytic CO$_2$ adsorption significantly influenced the catalytic activity, as well as the oxygen species formed by the dissociation of the CO$_2$ molecules, and suppressed carbon deposition [16]. The Ni/Al$_2$O$_3$ catalyst employing the acidic Al$_2$O$_3$ support showed low CO$_2$ desorption characteristics of 26 µmol/g (Table 1). The Ni/MgO catalyst presented a CO$_2$ desorption peak in the 100–700 °C temperature range, and exhibited the highest CO$_2$ desorption amount (170 µmol/g), owing to the basic properties of the MgO support. In addition, because Ni/MgO-Al$_2$O$_3$ and Ni/MgAl$_2$O$_4$ catalysts contained the alkaline earth metal Mg, they exhibited improved CO$_2$ adsorption properties compared to the Ni/Al$_2$O$_3$ catalyst. In particular, Ni/MgAl$_2$O$_4$, which had a high metal dispersion and large specific surface area, exhibited a higher CO$_2$ desorption amount (125 µmol/g) than the Ni/MgO-Al$_2$O$_3$ catalyst (110 µmol/g). Commercial catalyst A, which employed

the acidic Al_2O_3 support showed poor CO_2 adsorption properties, due to the formation of bulk NiO. The commercial catalyst B presented CO_2 desorption peaks at 200 and 500 °C, and an increased CO_2 desorption amount of 81 μmol/g compared to the catalysts that employed Al_2O_3 as a support, due to the presence of the alkaline earth metal Ca.


Figure 3. CO_2-TPD profiles of Ni catalysts with various supports.

2.2. Catalytic Test in DRM

The catalytic activity of the DRM reaction was evaluated in the temperature range of 600–750 °C, and the CH_4 and CO_2 conversions are presented in Figure 4. Since the DRM is an endothermic reaction, it exhibited high CH_4 and CO_2 conversions with increasing reaction temperature. The Ni/MgO catalyst, which formed a NiO-MgO solid solution, was reduced at temperatures above 1000 °C; therefore, the Ni/MgO catalyst did not show catalytic activity in the DRM reaction. Since the Ni/Al_2O_3 catalyst also formed a $NiAl_2O_4$ spinel, this resulted in low metal dispersion and low reducibility of the catalyst. For this reason, the Ni/Al_2O_3 catalyst showed a low CH_4 conversion (66%) at 750 °C, whereas, Ni/MgO-Al_2O_3 and Ni/$MgAl_2O_4$ catalysts exhibited high CH_4 conversions of 78 and 77%, respectively, compared with Ni/Al_2O_3. This is because of the high dispersion of the Ni metals due to the suppression of the formed $NiAl_2O_4$ and NiO-MgO solid solutions. On the other hand, commercial catalysts A and B showed low CH_4 conversions, due to the formation of bulk NiO, despite the presence of 15 wt% Ni metal. However, because the alkaline earth metal-containing commercial catalyst B formed a lower amount of $NiAl_2O_4$ compared with the commercial catalyst A, the catalyst B presented relatively high CH_4 and CO_2 conversions. This result indicates that the catalytic characteristics (such as metal dispersion and crystalline phase), which depend on the type of support employed, played an important role in determining the catalytic activity.

H_2 and CO yields and H_2/CO ratio are presented in Figure 4 and Table 2, respectively. The CO yield (56–86%) was higher than the H_2 yield (34–74%). In addition, the H_2/CO ratio of the produced syngas after the DRM reaction was 0.6–0.9. These results are attributed to the RWGS reaction (Equation (2)) as a side reaction, as mentioned above. Theoretically, the ratio of the H_2/CO produced in the DRM reaction (Equation (1)) is 1. However, the H_2/CO ratio was lower than 1, because the RWGS reaction occurs as a side reaction under the reaction conditions of the DRM process [29]. Among the tested catalysts, Ni/MgO-Al_2O_3 and Ni/$MgAl_2O_4$ presented ratios close to the equilibrium H_2/CO ratio of 0.9.

(a)

(b)

(c)

(d)
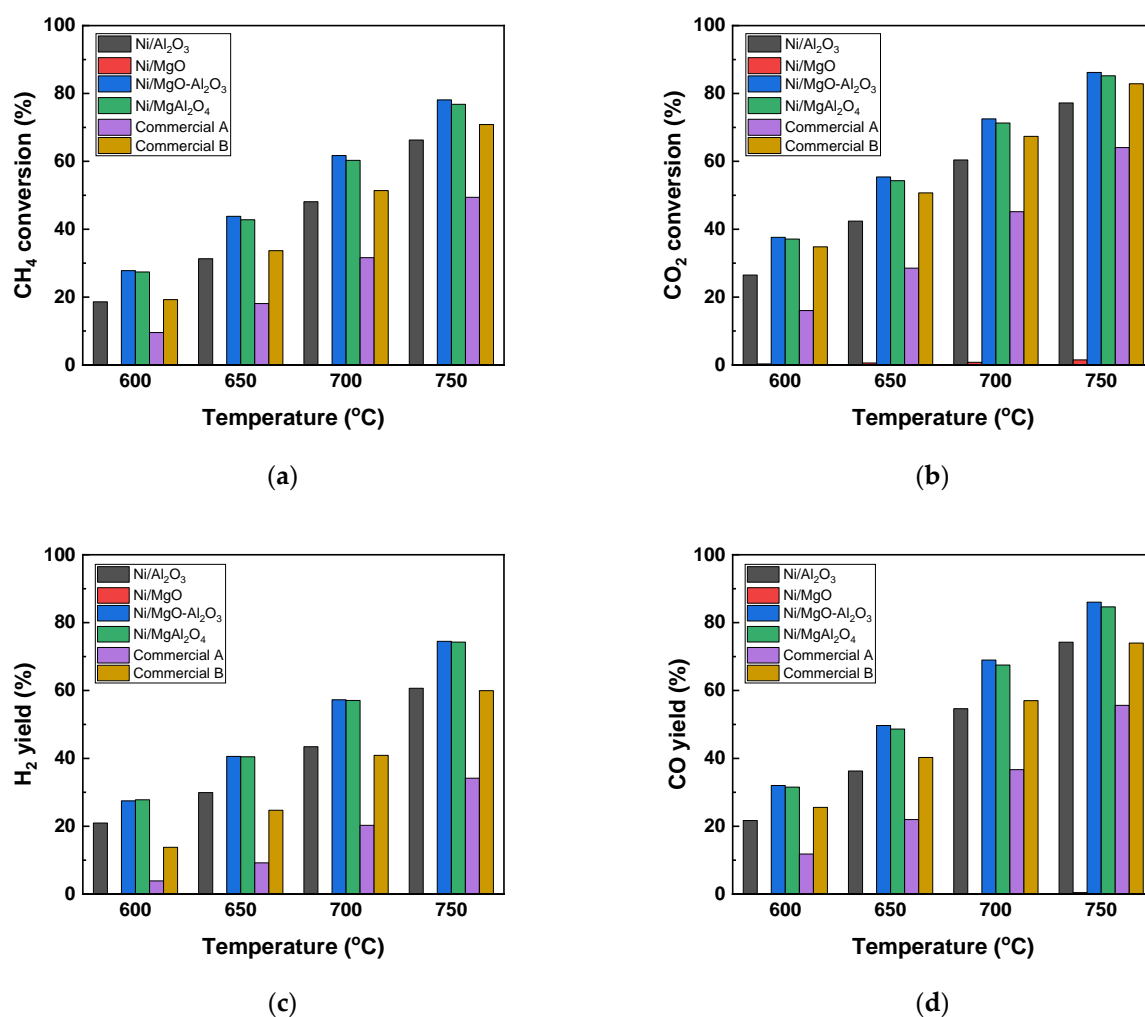
Figure 4. CH_4 conversion (**a**), CO_2 conversion (**b**), H_2 yield (**c**), and CO yield (**d**) with reaction temperature over Ni catalysts (reaction conditions: Temp. = 600–750 °C, $CH_4/CO_2/N_2$ = 1/1/1, GHSV = 144,000 mL/g_{cat}·h).

Table 2. H_2/CO ratio of Ni catalysts with various supports (reaction conditions: Temp. = 750 °C, $CH_4/CO_2/N_2$ = 1/1/1, GHSV = 144,000 mL/g_{cat}·h).

	Ni/Al$_2$O$_3$	Ni/MgO	Ni/MgO-Al$_2$O$_3$	Ni/MgAl$_2$O$_4$	Commercial A	Commercial B
H$_2$/CO ratio	0.8	N/A [1]	0.9	0.9	0.6	0.8

[1] N/A: Not available.

2.3. Coke Formation Study

    To investigate the stability of the reaction and coke resistance, a stability test was conducted in the absence of the diluent (Figure 5). Coke formation reactions of the CH_4 decomposition reaction (Equation (3)) and CO disproportionation reaction (Equation (4)) occur simultaneously in the temperature range of 557–700 °C [10]. Thus, stability tests were performed at 600 °C and a TOS of 20 h. As the Ni/MgO catalyst did not exhibit catalytic activity in the catalytic test, in accordance with the reaction temperature, a stability test was conducted, except for the Ni/MgO catalyst. The Ni/Al$_2$O$_3$ catalyst tended toward constantly reduced CH_4 and CO_2 conversions over 20 h. The Ni/Al$_2$O$_3$ catalyst had 21% of the initial CH_4 conversion, the Ni/Al$_2$O$_3$ catalyst decreased to 16% of CH_4 conversion after 20 h. Ni/MgO-Al$_2$O$_3$ and Ni/MgAl$_2$O$_4$ catalysts, which added the Mg alkaline earth

metal, had high CH_4 and CO_2 conversions compared to the Ni/Al_2O_3 catalyst, owing to the improved reducibility of the catalyst and high metal dispersion. In particular, the $Ni/MgO-Al_2O_3$ and $Ni/MgAl_2O_4$ catalysts showed higher CH_4 and CO_2 conversions than the commercial catalyst A. On the other hand, the commercial catalyst B exhibited a CH_4 conversion of 20–22%, and had a higher CH_4 conversion than the catalyst that employed Al_2O_3 as a support.

(**a**)

(**b**)
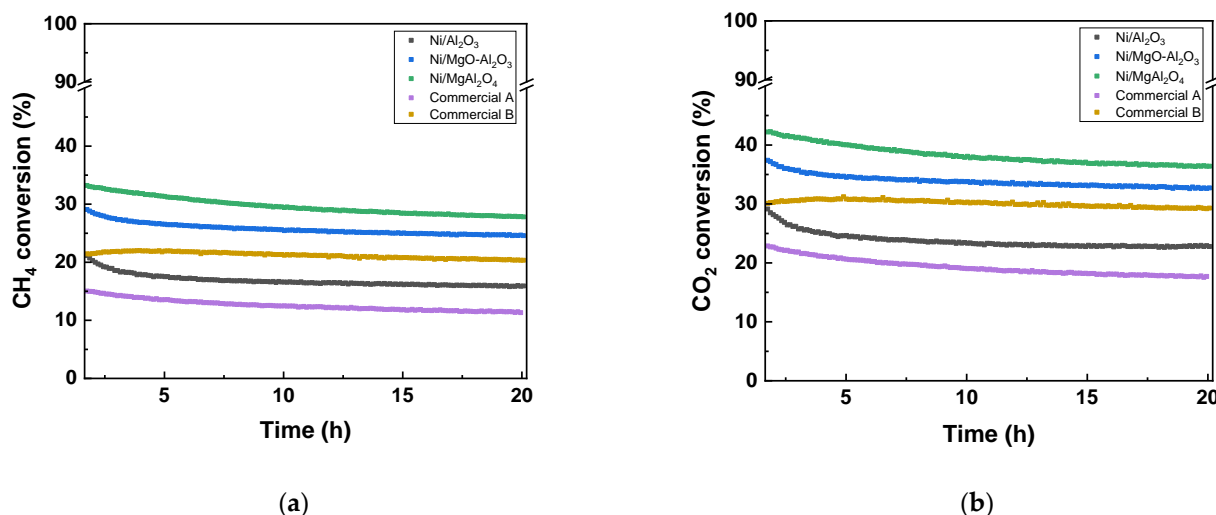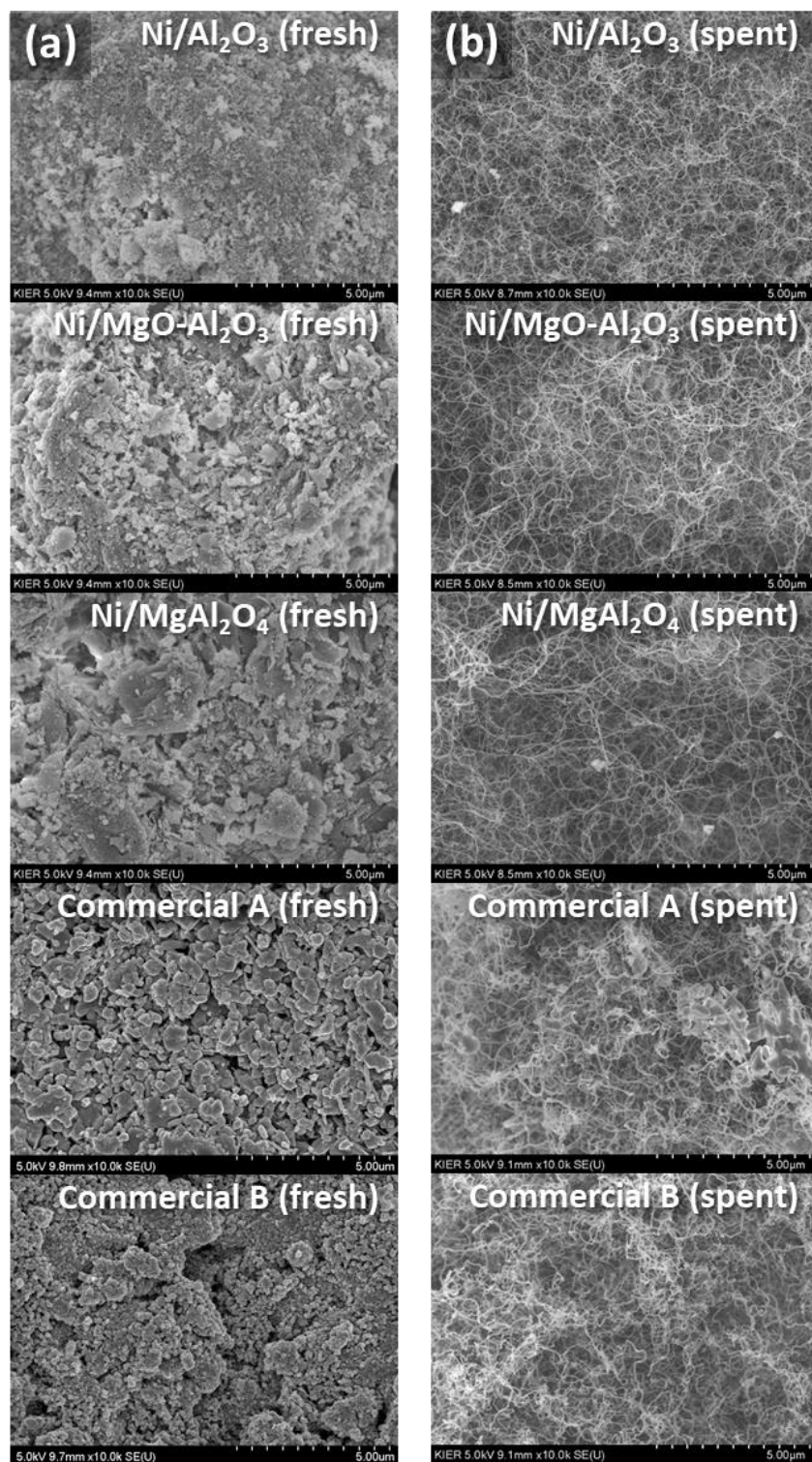
Figure 5. CH_4 conversion (**a**) and CO_2 conversion (**b**) with long-term test over Ni catalysts (reaction conditions: Temp. = 600 °C, $CH_4/CO_2/N_2$ = 1/1/1, GHSV = 144,000 mL/g_{cat}·h, TOS = 20 h).

To investigate the carbon formed on the surface of the catalyst, SEM and TGA analyses were performed on the recovered spent catalysts. The morphologies of the formed carbon were analyzed using SEM images, as shown in Figure 6. Sehested reported that three types of carbon were formed during reforming reactions: pyrolytic carbon, encapsulating carbon, and filamentous carbon [30]. Pyrolytic carbon is formed at temperatures higher than 600 °C, owing to thermal decomposition of hydrocarbon compounds. Since the encapsulating carbon covered particles of the catalyst, it caused immediate catalyst deactivation. Filamentous carbon is formed and grown between the Ni particles and the support, which causes catalyst pore plugging. For this reason, filamentous carbon results in catalyst deactivation, causing catalyst destruction and a pressure drop. The formation of filamentous carbon was also confirmed on the surface of the spent catalysts after the stability test, and SEM images of all the analyzed catalysts indicated the formation of a large amount of filamentous carbon on the catalyst surface.

Quantitative analysis of the amount of deposited carbon was performed through weight loss analysis using TGA up to 800 °C. The TGA results are shown in Figure 7 and Table 3. The weight loss of the spent catalyst was classified according to the temperature range; desorption of H_2O and CO_2 occurred in the temperature range of 250–300 °C, and the oxidation of carbon due to the release of CO and CO_2 occurred in the temperature range of 480–640 °C [31]. In addition, graphitic filamentous carbon is mainly oxidized at a high temperature of 530 °C [32]. Quantitative analysis of the formed carbon was performed using the recovered spent catalysts containing alkaline earth metals, which showed a relatively high catalytic activity during the stability test. Results from the TG profiles indicated that most of the weight loss of the spent catalysts occurred at temperatures above 500 °C. The amount of deposited carbon was calculated from the weight loss, in the temperature range of 50–800 °C (Table 3). The amount of deposited carbon on the $Ni/MgO-Al_2O_3$ and $Ni/MgAl_2O_4$ catalysts was 21.4 and 29.3 wt%, respectively. In comparison, the commercial catalyst B contained twice the amount of deposited carbon (47.1 wt%). These results are related to the CO_2 adsorption characteristics of the catalysts [33]. Since CO_2 is an acidic gas, CO_2 adsorption was enhanced by the addition of basic materials, such as Mg and Ca.

In addition, oxygen species produced by the dissociation of CO_2 molecules are used in the oxidation of deposited carbon on the catalyst surface. Therefore, increasing the basic properties of the DRM catalyst could improve catalyst durability. Therefore, commercial catalyst B, which showed relatively low CO_2 adsorption properties (81 μmol/g), contained a large amount of carbon compared to the $Ni/MgO-Al_2O_3$ and $Ni/MgAl_2O_4$ catalysts, which had high CO_2 adsorption properties, of 110 and 125 μmol/g, respectively.

Figure 6. SEM images of fresh (**a**) and spent (**b**) catalysts with various supports (reaction conditions: Temp. = 600 °C, $CH_4/CO_2/N_2$ = 1/1/1, GHSV = 144,000 mL/g_{cat}·h, TOS = 20 h).
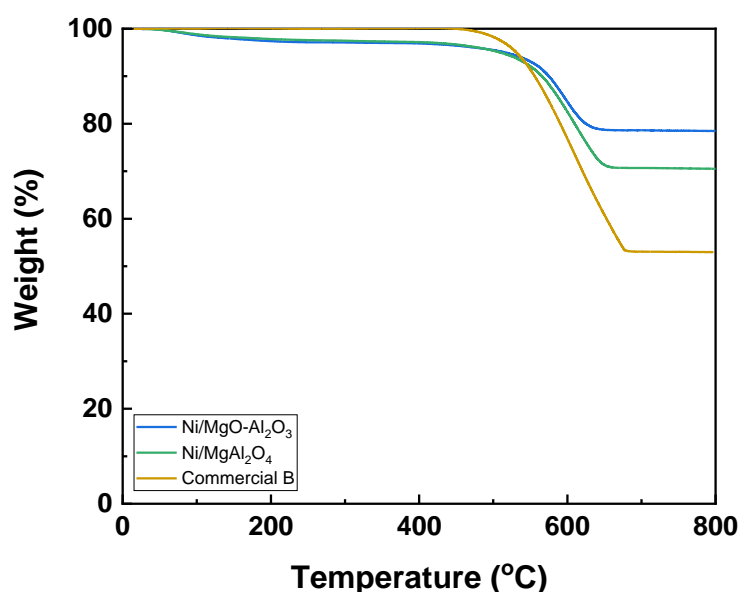
Figure 7. TG profiles of spent catalysts under air (reaction conditions: Temp. = 600 °C, $CH_4/CO_2/N_2 = 1/1/1$, GHSV = 144,000 mL/g_{cat}·h, TOS = 20 h).

Table 3. Amount of coke over Ni catalysts from TG profiles (reaction conditions: Temp. = 600 °C, $CH_4/CO_2/N_2 = 1/1/1$, GHSV = 144,000 mL/g_{cat}·h, TOS = 20 h).

Catalysts	Amount of Coke [1] [wt%]
Ni/MgO-Al$_2$O$_3$	21.4
Ni/MgAl$_2$O$_4$	29.3
Commercial B	47.1

[1] Calculated from the following equation; (Amount of coke) $= \frac{(sample\ weight\ at\ 50\ °C) - (sample\ weight\ at\ 800\ °C)}{(sample\ weight\ at\ 50\ °C)} \times 100$.

3. Materials and Methods

3.1. Materials

Ni(NO$_3$)$_2$·6H$_2$O (97%, Junsei) was used as the active metal precursor; γ-Al$_2$O$_3$ (PU-RALOX TH 100/150, SASOL), MgO (≥99%, Sigma-Aldrich), MgO-Al$_2$O$_3$ hydrotalcite (MgO:Al$_2$O$_3$ = 30:70, SASOL), and MgAl$_2$O$_4$ (MG30 pre-calcined at 800 °C, SASOL) were used as supports for the Ni-based catalyst. Ni-based commercial catalysts Ni/Al$_2$O$_3$ (FCR-4; Clariant) and Ni/CaAl$_2$O$_4$ (R-70; Clariant)) were used as reference catalysts.

3.2. Catalyst Preparation

Ni-based catalysts were prepared using the incipient wetness impregnation method. Nickel nitrate was dissolved in distilled water and impregnated with γ-Al$_2$O$_3$. The prepared Ni/Al$_2$O$_3$ catalyst was dried overnight at room temperature, followed by calcination at 800 °C for 6 h in air. Ni/MgO, Ni/MgO-Al$_2$O$_3$, and Ni/MgAl$_2$O$_4$ catalysts were also prepared by the same method, and 10 wt% Ni active metal was supported on the catalysts.

3.3. Characteristics

The active metal content supported on the catalyst was analyzed using inductively coupled plasma-optical emission spectroscopy (ICP-OES, AVIO500, Perkin Elmer). The crystalline phases and composition of the catalysts were analyzed using an X-ray diffractometer (XRD, SmartLab High Temp, Rigaku, Tokyo, Japan). Diffraction peaks were obtained in the 2θ range of 10–90° with a step size of 0.02°. The specific surface area and pore size distribution of the catalyst were obtained using the Brunauer–Emmett–Teller and BarrettJoyner–Halenda methods (BET-BJH, BELSORP-MAX, MicrotracBEL Corp., Osaka, Japan). A sample (0.2 g) was pretreated at 300 °C for 3 h. N$_2$ adsorption/desorption

isotherms and pore size distributions were analyzed at -196 °C using liquid nitrogen. H_2-chemisorption (BEL-METAL-3, MicrotracBEL Corp., Osaka, Japan) was performed to determine the metal dispersion of the catalyst. The sample (50 mg) was reduced at 700 °C for 2 h under H_2 flow, and H_2 gas was adsorbed at 50 °C using 20% H_2/Ar gas. H_2-temperature programmed reduction (H_2-TPR, BELCAT-B, MicrotracBEL Corp., Osaka, Japan) analysis was performed to investigate the reducibility of the catalyst and the interaction between the active metal and support. The analysis was performed by increasing the temperature up to 1000 °C (10 °C/min) under 10% H_2/Ar flow using a 50 mg sample. The CO_2 adsorption properties were analyzed through CO_2-temperature programmed desorption (CO_2-TPD, BELCAT-B, MicrotracBEL Corp., Osaka, Japan) analysis. The sample (50 mg) was reduced at 700 °C for 2 h under 10% H_2/Ar flow. The CO_2 was adsorbed at 50 °C using 10% CO_2/He gas and desorbed by increasing the temperature to 800 °C (10 °C/min). In addition, the morphology of the formed carbon in the spent catalysts was analyzed using scanning electron microscope (SEM, Regulus 8220, HITACHI, Tokyo, Japan) analysis. Quantitative analysis of carbon on the spent catalysts was performed using thermogravimetric analysis (TGA, TGA 92-18, Setaram, Caluire-et-Cuire, France). The weight loss was measured by loading 7 mg of the sample. The sample was oxidized by increasing the temperature to 800 °C at 10 °C/min in air.

3.4. Catalytic Tests

Catalytic activity was evaluated in a fixed bed reactor system. The 3/8″ quartz reactor was filled with a catalyst (50 mg, 150–250 μm) and 1100 °C pre-calcined $MgAl_2O_4$ as a diluent (500 mg, 150–250 μm) in a ratio of 1:10. Before the catalytic test, the catalyst was reduced at 700 °C for 2 h with 10 vol.% H_2/N_2 gas. The evaluation of the catalytic activity was performed in a temperature range of 600–750 °C. The feeds of CH_4, CO_2, and N_2 were injected to equal ratio. The total flow rate was 120 mL/min, and GHSV corresponded to 144,000 mL/g_{cat}·h. The reaction temperature was controlled using a K-type thermocouple (TC), the TC was located inside the catalyst layer. The produced gas was detected using a micro-gas chromatograph (3000A Micro GC, Agilent, CA, USA) equipped with a thermal conductivity detector (TCD) using MolSeive 5A and PlotU columns.

4. Conclusions

DRM reaction over Ni-based catalysts was studied as a function of the type of catalyst support used (Al_2O_3, MgO, MgO-Al_2O_3 (LDH), and $MgAl_2O_4$ (spinel)). The type of support significantly influenced the reducibility and metal dispersion of the Ni-based catalysts. The Ni/Al_2O_3 and Ni/MgO catalysts had low metal dispersion, due to the formation of $NiAl_2O_4$ and NiO-MgO solid solutions, respectively. In addition, these catalysts had a strong interaction between the Ni active metal and support, indicated by the high temperature (more than 900 °C) required for reduction. In contrast, Ni/MgO-Al_2O_3 and Ni/$MgAl_2O_4$ catalysts suppressed the formation of $NiAl_2O_4$ and NiO-MgO solid solutions, exhibited high metal dispersion, and were reduced at lower temperatures compared with the Ni/Al_2O_3 and Ni/MgO catalysts. Moreover, Ni/MgO-Al_2O_3 and Ni/$MgAl_2O_4$ catalysts containing Mg had enhanced CO_2 adsorption properties. In the DRM reaction, Ni/MgO-Al_2O_3 and Ni/$MgAl_2O_4$ catalysts exhibited high CH_4 conversion (>75%) at 750 °C compared to commercial catalysts. Furthermore, Ni/MgO-Al_2O_3 and Ni/$MgAl_2O_4$ catalysts showed enhanced coke resistance compared to commercial catalyst B. Therefore, the metal dispersion, basic properties, and metal-support interaction of the catalyst in accordance with the type of support were confirmed to significantly influence the catalyst performance in the DRM reaction.

Author Contributions: Conceptualization, U.H.J. and K.Y.K.; methodology, D.H.S.; formal analysis, Y.E.K. and H.B.I.; data curation, T.H.L.; writing-original draft preparation, D.H.S.; writing—review and editing, K.Y.K.; supervision, K.Y.K. and K.B.L.; project administration, U.H.J. All authors have read and agreed to the published version of the manuscript.

References

1. Subramanian, S.; Song, Y.; Kim, D.; Yavuz, C.T. Redox and nonredox CO_2 utilization: Dry reforming of methane and catalytic cyclic carbonate formation. *ACS Energy Lett.* **2020**, *5*, 1689–1700. [CrossRef]
2. Parsapur, R.K.; Chatterjee, S.; Huang, K.-W. The insignificant role of dry reforming of methane in CO_2 emission relief. *ACS Energy Lett.* **2020**, *5*, 2881–2885. [CrossRef]
3. San-José-Alonso, D.; Juan-Juan, J.; Illán-Gómez, M.; Román-Martínez, M. Ni, Co and bimetallic Ni–Co catalysts for the dry reforming of methane. *Appl. Catal. A* **2009**, *371*, 54–59. [CrossRef]
4. Edwards, J.; Maitra, A. The chemistry of methane reforming with carbon dioxide and its current and potential applications. *Fuel Process. Technol.* **1995**, *42*, 269–289. [CrossRef]
5. Zhang, M.; Shengfu, J.; Linhua, H.; Fengxiang, Y.; Chengyue, L.; Hui, L. Structural characterization of highly stable Ni/SBA-15 catalyst and its catalytic performance for methane reforming with CO_2. *Chin. J. Catal.* **2006**, *27*, 777–781. [CrossRef]
6. Arora, S.; Prasad, R. An overview on dry reforming of methane: Strategies to reduce carbonaceous deactivation of catalysts. *RSC Adv.* **2016**, *6*, 108668–108688. [CrossRef]
7. Abdullah, B.; Abd Ghani, N.A.; Vo, D.-V.N. Recent advances in dry reforming of methane over Ni-based catalysts. *J. Clean. Prod.* **2017**, *162*, 170–185. [CrossRef]
8. Budiman, A.W.; Song, S.-H.; Chang, T.-S.; Shin, C.-H.; Choi, M.-J. Dry reforming of methane over cobalt catalysts: A literature review of catalyst development. *Catal. Surv. Asia* **2012**, *16*, 183–197. [CrossRef]
9. Praserthdam, S.; Somdee, S.; Rittiruam, M.; Balbuena, P.B. Computational study of the evolution of Ni-based catalysts during the dry reforming of methane. *Energy Fuels* **2020**, *34*, 4855–4864. [CrossRef]
10. Wang, S.; Lu, G.; Millar, G.J. Carbon dioxide reforming of methane to produce synthesis gas over metal-supported catalysts: State of the art. *Energy Fuels* **1996**, *10*, 896–904. [CrossRef]
11. Ginsburg, J.M.; Piña, J.; El Solh, T.; De Lasa, H.I. Coke formation over a nickel catalyst under methane dry reforming conditions: Thermodynamic and kinetic models. *Ind. Eng. Chem. Res.* **2005**, *44*, 4846–4854. [CrossRef]
12. ZHANG, R.-j.; XIA, G.-f.; LI, M.-f.; Yu, W.; Hong, N.; LI, D.-d. Effect of support on the performance of Ni-based catalyst in methane dry reforming. *J. Fuel Chem. Technol.* **2015**, *43*, 1359–1365. [CrossRef]
13. Rezaei, M.; Alavi, S.; Sahebdelfar, S.; Bai, P.; Liu, X.; Yan, Z.-F. CO_2 reforming of CH_4 over nanocrystalline zirconia-supported nickel catalysts. *Appl. Catal. B* **2008**, *77*, 346–354. [CrossRef]
14. Bychkov, V.Y.; Tyulenin, Y.P.; Firsova, A.; Shafranovsky, E.; Gorenberg, A.Y.; Korchak, V. Carbonization of nickel catalysts and its effect on methane dry reforming. *Appl. Catal. A* **2013**, *453*, 71–79. [CrossRef]
15. Li, Y.; Lu, G.; Ma, J. Highly active and stable nano NiO–MgO catalyst encapsulated by silica with a core–shell structure for CO_2 methanation. *RSC Adv.* **2014**, *4*, 17420–17428. [CrossRef]
16. Tomishige, K.; Yamazaki, O.; Chen, Y.; Yokoyama, K.; Li, X.; Fujimoto, K. Development of ultra-stable Ni catalysts for CO_2 reforming of methane. *Catal. Today* **1998**, *45*, 35–39. [CrossRef]
17. Özdemir, H.; Öksüzömer, M.F.; Gürkaynak, M.A. Preparation and characterization of Ni based catalysts for the catalytic partial oxidation of methane: Effect of support basicity on H_2/CO ratio and carbon deposition. *Int. J. Hydrog. Energy* **2010**, *35*, 12147–12160. [CrossRef]
18. Bobadilla, L.; Garcilaso, V.; Centeno, M.; Odriozola, J. CO_2 reforming of methane over Ni-Ru supported catalysts: On the nature of active sites by operando DRIFTS study. *J. CO2 Util.* **2018**, *24*, 509–515.
19. Koo, K.Y.; Roh, H.-S.; Seo, Y.T.; Seo, D.J.; Yoon, W.L.; Park, S.B. Coke study on MgO-promoted Ni/Al_2O_3 catalyst in combined H_2O and CO_2 reforming of methane for gas to liquid (GTL) process. *Appl. Catal. A* **2008**, *340*, 183–190. [CrossRef]
20. Djaidja, A.; Libs, S.; Kiennemann, A.; Barama, A. Characterization and activity in dry reforming of methane on NiMg/Al and Ni/MgO catalysts. *Catal. Today* **2006**, *113*, 194–200. [CrossRef]
21. Gao, X.; Ge, Z.; Zhu, G.; Wang, Z.; Ashok, J.; Kawi, S. Anti-coking and anti-sintering Ni/Al_2O_3 catalysts in the dry reforming of methane: Recent progress and prospects. *Catalysts* **2021**, *11*, 1003. [CrossRef]
22. Zanganeh, R.; Rezaei, M.; Zamaniyan, A. Preparation of nanocrystalline NiO–MgO solid solution powders as catalyst for methane reforming with carbon dioxide: Effect of preparation conditions. *Adv. Powder Technol.* **2014**, *25*, 1111–1117. [CrossRef]
23. Nurunnabi, M.; Li, B.; Kunimori, K.; Suzuki, K.; Fujimoto, K.-I.; Tomishige, K. Performance of NiO–MgO solid solution-supported Pt catalysts in oxidative steam reforming of methane. *Appl. Catal. A* **2005**, *292*, 272–280. [CrossRef]
24. Mori, H.; Wen, C.-j.; Otomo, J.; Eguchi, K.; Takahashi, H. Investigation of the interaction between NiO and yttria-stabilized zirconia (YSZ) in the NiO/YSZ composite by temperature-programmed reduction technique. *Appl. Catal. A* **2003**, *245*, 79–85. [CrossRef]

25. Becerra, A.M.; Castro-Luna, A.E. An investigation on the presence of $NiAl_2O_4$ in a stable Ni on alumina catalyst for dry reforming. *J. Chil. Chem. Soc.* **2005**, *50*, 465–469. [CrossRef]

26. Guo, J.; Lou, H.; Zhao, H.; Chai, D.; Zheng, X. Dry reforming of methane over nickel catalysts supported on magnesium aluminate spinels. *Appl. Catal. A* **2004**, *273*, 75–82. [CrossRef]

27. Alipour, Z.; Rezaei, M.; Meshkani, F. Effect of alkaline earth promoters (MgO, CaO, and BaO) on the activity and coke formation of Ni catalysts supported on nanocrystalline Al_2O_3 in dry reforming of methane. *J. Ind. Eng. Chem.* **2014**, *20*, 2858–2863. [CrossRef]

28. Gao, J.; Jia, C.; Zhang, M.; Gu, F.; Xu, G.; Su, F. Effect of nickel nanoparticle size in Ni/α-Al_2O_3 on CO methanation reaction for the production of synthetic natural gas. *Catal. Sci. Technol.* **2013**, *3*, 2009–2015. [CrossRef]

29. Serrano-Lotina, A.; Daza, L. Influence of the operating parameters over dry reforming of methane to syngas. *Int. J. Hydrog. Energy* **2014**, *39*, 4089–4094. [CrossRef]

30. Sehested, J. Four challenges for nickel steam-reforming catalysts. *Catal. Today* **2006**, *111*, 103–110. [CrossRef]

31. Tsyganok, A.I.; Tsunoda, T.; Hamakawa, S.; Suzuki, K.; Takehira, K.; Hayakawa, T. Dry reforming of methane over catalysts derived from nickel-containing Mg–Al layered double hydroxides. *J. Catal.* **2003**, *213*, 191–203. [CrossRef]

32. Wang, S.; Lu, G.Q. Effects of promoters on catalytic activity and carbon deposition of Ni/γ-Al_2O_3 catalysts in CO_2 reforming of CH_4. *J. Chem. Technol. Biotechnol.* **2000**, *75*, 589–595. [CrossRef]

33. Singha, R.K.; Yadav, A.; Agrawal, A.; Shukla, A.; Adak, S.; Sasaki, T.; Bal, R. Synthesis of highly coke resistant Ni nanoparticles supported MgO/ZnO catalyst for reforming of methane with carbon dioxide. *Appl. Catal. B* **2016**, *191*, 165–178. [CrossRef]